Wetting of bio-rejuvenator nanodroplets on bitumen: A molecular dynamics investigation

Haiqin Xu [a,b], Yingxue Zou [a], Gordon Airey [b], Haopeng Wang [c] , Hanyu Zhang [b], Shaopeng Wu [a,*], Anqi Chen [a,*]

[a] State Key Laboratory of Silicate Materials for Architectures, Wuhan University of Technology, Wuhan 430070, China;

[b] Nottingham Transportation Engineering Centre, Faculty of Engineering, University of Nottingham, University Park, Nottingham NG7 2RD, UK;

[c] Department of Civil and Environmental Engineering, University of Liverpool, Liverpool, L69 3BX, UK

* Correspondence author: wusp@whut.edu.cn (S. Wu), anqi.chen@whut.edu.cn (A. Chen).

ABSTRACT

Wetting is the first step during the mix process between rejuvenator and bitumen, which is important for mix efficiency and performance recovery. The wetting of bio-rejuvenator nanodroplets on bitumen was investigated by molecular dynamics (MD) simulations in this research. The bitumen molecule model and bio-rejuvenator nanodroplets were firstly built, then bio-rejuvenator nanodroplets/bitumen interface wetting model were assembled and constructed. Different simulated temperatures were applied to reach equilibrium in the wetting process. Dynamic wetting phenomenon, contact angle of nanodroplets, dynamic movement of nanodroplets, interaction between nanodroplets and bitumen, and hysteresis of contact angle were characterized respectively. The results show that the bio-rejuvenator nanodroplets will first approach the bitumen quickly, and then slow down to an equilibrium state in the wetting process, which delayed 1 ns with energy equilibrium independently. Its contact angle would decrease crossing 90 degrees with time, the equilibrium contact angle of which varies linearly with simulated temperature. The time of nanodroplets reaching partial wetting state decreased with the increment of temperature, but complete wetting state was hard to reach even if the temperature was 433 K. During the nanodroplets movement, contact linear velocity of precursor film and cosine of contact angle was linearly related after nanodroplets and bitumen had caught each other. It was also found that the increasing mix degree was supported by the combination of wetting and infiltration before 373 K and by wetting mainly after 373 K. Finally, the application of external force on bio-rejuvenator nanodroplets will cause hysteresis

phenomenon and it can be weakened by higher temperature.

Key words: Wetting, Rejuvenator, Nanodroplets, MD, Bitumen

1 Introduction

Highway transportation, widely considered as one of the most important parts of the transportation system, is occupying the vital position in the whole transportation industry. Due to the outstanding characteristics of asphalt concrete for service which includes comfort driving, low noise, superior skid resistance, simplicity of maintenance, more than 90% of roads in Europe are constructed with asphalt concrete (Yang et al., 2023; Zhao et al., 2024; Hu et al., 2022), where it supports 80% of passenger transportation and 70% of inland cargo transportation (European Commission. Directorate General for Regional and Urban Policy., 2022; European Union Road Federation (ERF), 2014). In China, there are also over 1.2 million kilometers of asphalt concrete pavement to maintain the transportation system (Xu et al., 2022b). With the globalization of trade and economic recovery in the recent years, additional road infrastructure will be needed to undertake the transportation tasks, especially the pavement. According to the official report by the Ministry of Transport of the People's Republic of China, the road length for transportation has increased over 10% during the past five years in China (Ministry of Transport of the People's Republic of China, 2023). However, since the pavement was built, it will be exposed to the aging of heavy sunshine, moist weather and continuous loading (Li et al., 2020; Xu et al., 2022a; Zou et al., 2021). The occurrence of aging will oxidize and harden the bitumen and then result in various deterioration in the pavement such as raveling, cracking, and rutting (Cui et al., 2021). Unfortunately, bitumen materials can't recover to the original state spontaneously (Yang et al., 2022a). If the aging asphalt concrete can't be regenerated, the pavement that exceeds the service life will become unsolvable waste, which not only wastes a lot of resources but also causes incalculable damage to the environment (Yang et al., 2022b). Therefore, the application of rejuvenator materials for performance recovery of bitumen has become the appropriate determination for the pavement engineering.

Rejuvenator is the material that can soft bitumen, recover the properties of bitumen and even connect the broken bonds (Cao et al., 2020). Currently, countless rejuvenators are mainly composed of bio-oil (including sunflower oil, palm oil), waste oil (like cooking oil and engine oil), petroleum-based product, and even soft bitumen (Rathore et al., 2022; Zhao et al., 2022). As shown in Figure 1, the rejuvenators have been widely applied in pavement engineering of researches and practical projects. The most commonly application of rejuvenators in pavement engineering is the recycling projects of reclaimed asphalt pavement (RAP) (Ziari et al., 2022). The rejuvenators will be always added into asphalt mixture directly during the mixing process to mix with the aging bitumen. The fusion will be continuing during the paving process until it returns to normal temperature. Rejuvenators are also used in maintenance projects widely like fog seal wheret the rejuvenators is mixed with the aging bitumen on the pavement by spraying (Cui et al., 2019; Tian et al., 2021). It requires high permeability of rejuvenators to penetrate into bitumen and asphalt concrete pavement. Furthermore, some in-situ regeneration technologies have been developed in the recent years. The rejuvenators would be encapsulated in the capsule and fibers (Shu et al., 2020; Yu et al., 2022; Zhang et al., 2019). Once stress at the crack tip or repeated load is applied to the encapsulation, the rejuvenators will be released, and filled the crack to diffuse on the bitumen. Apart from the release of rejuvenators by force induced at ordinary temperature, it can also be released by the temperature changing (Wan et al., 2022). The conductive materials are added into the encapsulation material for generating heat under the electric and magnetic fields (Tabaković et al., 2022; Wan et al., 2021). The heat will induce the encapsulation material to shrink or crack to release the rejuvenators (X. Wang et al., 2018). Meanwhile, the release mechanism of rejuvenators in the combination of induction heating technology and encapsulation method is similar (Xu et al., 2021). Numerous kinds and application scenarios of rejuvenators make the reasonably selection of rejuvenators so difficult. It is the basis of reasonable selection of rejuvenators to clarify the action mechanism between rejuvenators and bitumen. Correspondingly, the researches on the mixing process of rejuvenators and bitumen become popular and attractive.

Figure 1. The commonly application rejuvenators in pavement engineering

The mixing process of rejuvenators and bitumen can be commonly divided into wetting, diffusion, and fusion accompanied with infiltration. Karlsson et al. have used Fourier transform infrared spectroscopy by attenuated total reflectance (FTIR-ATR) and dynamic shear rheometer (DSR) to investigate diffusion of rejuvenators on bitumen and the result indicates the rates of diffusion detected by the DSR are of the same magnitude (Karlsson et al., 2007; Karlsson and Isacsson, 2003). Su et al. have also used FTIR-ATR method to evaluat diffusion behaviors of microencapsulated rejuvenator in aged bitumen (Su et al., 2016). Wang et al. have studied on the diffusion between rejuvenator and aged asphalt, and proposed three indexes to comparatively analyze the diffusion rate of different rejuvenators on aged asphalt effectively (Z. Wang et al., 2018). Xiao et al. have established a fast and visible detecting methods to characterize the diffusion process of rejuvenator oil in aged asphalt binder by image thresholding and GC-MS tracer analysis (Xiao et al., 2017). Li et al. have evaluated the diffusion efficiency of the rejuvenator and proved the benefits of higher temperature and longer time (Li Haibin et al., 2021). Fang et al. have investigated wetting behavior of four rejuvenators and their influencing factors of rejuvenator/old asphalt interface and found that wettability was affected by the interaction of temperature, surface tension, contact angle, viscosity and aging degree of bitumen in RAP (Fang et al., 2022). Molecular dynamic (MD) simulation was also widely used in the interaction between rejuvenators and bitumen, and the wetting phenomenon between liquid and matrix. Ding et al. have used the free volume theory to predict of the rejuvenator diffusion coefficient in aged bitumen (Ding et al., 2022). Xu and Zhang have explored the fusion and diffusion behaviors of rejuvenator in aged asphalt by molecular dynamics simulation (Xu et al., 2019; Zhan et al., 2022). Wang et al. have selected waste cooking oil, waste vegetable oil and waste engine oil as the rejuvenators to investigate the diffusion and fusion of virgin and aged asphalt generates the weak interface under stress concentration (Wang et al., 2022). However, it can be found that the previous researches focused on the diffusion and fusion process of the mix of rejuvenators and bitumen, while little attention was paid to the wetting process.

Therefore, for the research gap that the wetting process between rejuvenators and bitumen is still not known, the main objectives of this research were to investigate the dynamic wetting process of rejuvenators on the bitumen by molecular dynamics simulation. The bitumen model and bio-rejuvernator model (linoleic acid, $C_{18}H_{32}O_2$) were built firstly. Then bio-rejuvenator/bitumen interface wetting model were constructed, and different simulated temperatures were applied to reach equilibrium in the wetting process. The wetting process would be characterized by geometric trajectory and energy evaluation firstly. The contact angles of the nanodroplets were analyzed to evaluate the wetting statement. Then wetting dynamics of nanodroplets were quantified by atom number density and contact line velocity. Diffusion coefficient, adhesion work and infiltration work were also calculated. Finally, the hysteresis of contact angles by external force and temperature were analyzed.

2 Molecular dynamic simulation models

2.1 Bitumen model

Bitumen is the by-product of the crude oil refining industry, which is produced by the separation of light fractions from heavy crude oil. The process would make that bitumen is the typical hydrocarbon mixture that consists of a variety of functional groups and atoms such as oxygen, nitrogen, and sulfur. Consequently, it is so hard to provide a detailed explanation of components and structures of bitumen. Based on the different molecular sizes and solubility of the frictions, bitumen can be classified into four components (asphaltene, saturate, aromatic, and resin) that can be represented by one or more molecules to form the molecular model for bitumen. As shown in the Table 1, there are 12 components in the AAA-1 bitumen model held by Li and Greenfield and it is one of the most advanced and widely accepted asphalt models in the field of asphalt molecular simulation (Li and Greenfield, 2014; Xu et al., 2023). Compared with previous models, the 12-molecule bitumen model is more recognized for the reason that it is highly consistent with real bitumen in physical and chemical properties (Jennings and National Research Council, 1993; You et al., 2020). Therefore, the AAA-1 bitumen model was selected in this research, and Table 1 lists the parameters of represented components in detail.

Materials studio software was used for the model establishment and thermodynamic properties calculation for the bitumen model. 12-components molecules models for bitumen were built in 3D Atomistic tools. Condensed-phase optimized molecular potentials for atomistic simulation studies (COMPASS) was selected as the force field in this research, which can predict and calculate the structure and thermophysical properties of common inorganic and organic system over a large temperature and pressure range. The model was constructed with the following step: Firstly, the model was constructed by Amorphous Cell tools with an initial density of 0.1 g/cm^3 under the three-dimensional cycle condition in accordance with the proportion shown in Table 1. The geometric optimization with 5000 iterations was followed to eliminate unreasonable configurations in the model, leveling off the energy of the molecule to reach minimum energy. Then, Forcite tools was used to reach dynamic equilibrium for the stable structure and density, where a canonical ensemble (NVT, constant molecule number, model volume, and temperature) with 298 K, 1 fs time step for 100 ps and an isothermal-isobaric ensemble (NPT, constant atomic number, pressure, and temperature) with 298 K and 1.0 atm were conducted successively. The temperature and pressure of the block were controlled by Andersen barostat and Nose-Hoover-Langevin thermostat. Moreover, the Ewald with the accuracy of 0.001 kcal/mol and Atom-based with the cutoff distance of 15.5 Å are assigned as the Electrostatic and van der Waals summation method. Finally, the models have been established for further performance prediction and analysis in terms of thermodynamics parameters, structural characteristics, and dynamic behaviors. The rationality and reality of this model have been proved in our previous studies (Zou et al., 2024).

Table 1. Molecule compositions of bitumen and SARA frictions

Molecule	Chemical formula	Bitumen	
Squalene	$C_{30}H_{62}$	4	Saturate
Hopane	$C_{35}H_{62}$	4	
PHPN	$C_{35}H_{44}$	11	Aromatic
DOCHN	$C_{30}H_{46}$	13	

Quinolinohopane	$C_{40}H_{59}N$	4	
Thioisorenieratane	$C_{40}H_{60}S$	4	
Benzobisbenzothiophene	$C_{18}H_{10}S_2$	15	Resin
Pyridinohopane	$C_{36}H_{57}N$	4	
Trimethylbenzeneoxane	$C_{29}H_{50}O$	5	
Phenol	$C_{42}H_{54}O$	3	
Pyrrole	$C_{66}H_{81}N$	2	Asphaltene
Thiophene	$C_{51}H_{62}S$	3	

2.2 Bio-rejuvenator nanodroplets model

Linoleic acid ($C_{18}H_{32}O_2$), a polyunsaturated omega-6 fatty acid, was determined as the component of nanodroplets, which was proved as the main component with the highest measured content of bio-rejuvenator in the previous studies. Materials studio software was also used for the model establishment of bio-rejuvenator nanodroplets. The establishment steps of nanodroplets are shown in Figure 2, which is similar to that of bitumen model: Firstly, molecule chains of ($HOOC(CH_2)_7CH{=}CHCH_2CH{=}CH(CH_2)_4CH_3$) was modeled in the 3D Atomistic tools. The geometric optimization with 5000 iterations was conducted to level off the energy and obtain the reasonable model. Then, a cubic model was constructed by Amorphous Cell tools with the real density of 0.900 g/cm^3. The geometric optimization was conducted on the model. A canonical ensemble (NVT, constant molecule number, model volume, and temperature) with 298 K, 1 fs time step for 100 ps was followed to release the structure. Finally, the nanodroplets with 25 Å radius was obtained with nanocluster tool. Andersen barostat and Nose-Hoover-Langevin thermostat was used to control temporary and pressure. The Ewald with the accuracy of 0.001 kcal/mol and Atom-based with the cutoff distance of 15.5 Å are determined for Electrostatic and van der Waals summation method.

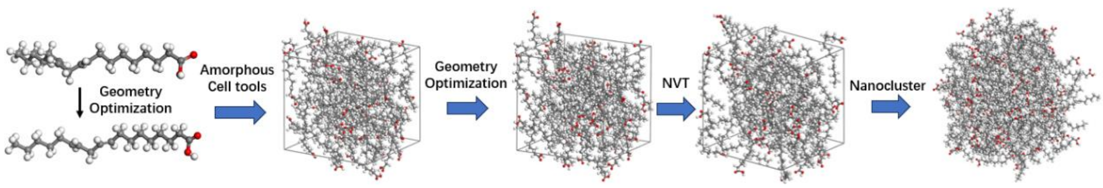

Figure 2. Bio-rejuvenator nanodroplets models

2.3 Bio-rejuvenator/bitumen interface wetting model

Before the combination of bitumen and nanodroplets, the lattice parameters of bitumen model were increased by 5 and 4 times in the X and Y directions respectively through Supercell tools. The bio-rejuvenator/bitumen interface wetting model was constructed by placing the nanodroplets on the center of bitumen surfaces with an interval of about 5 Å. Meanwhile, a 100 Å vacuum layer was set in the Z direction to prevent the influence of periodic structure. As shown in Figure 3, the model was eventually obtained.

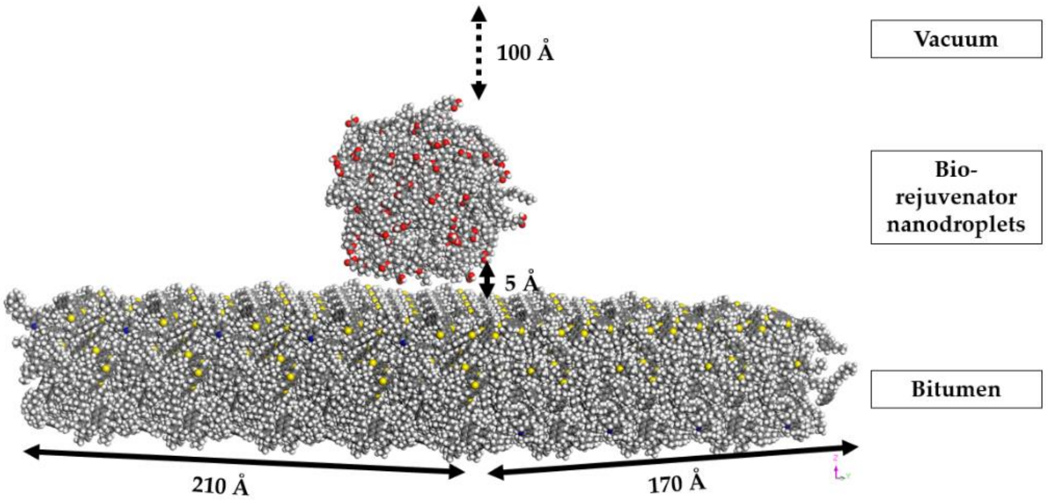

Figure 3. Schematic diagram of bio-rejuvenator nanodroplets/bitumen interface wetting model

3 Molecular dynamic simulation details

In this study, a classical molecular dynamics code: the large-scale atomic/molecular massively parallel simulator (LAMMPS) was used to perform the simulation. Scripts were used to import the interface models of bitumen and corrosion products in Materials studio software to LAMMPS and the chosen polymer consistent force field (PCFF) for simulation which has been validated to describe the organic, inorganic, and organic–inorganic interface systems. The force field is an empirical expression of the potential energy surface, and the total energy of the molecules is the sum of kinetic energy and potential energy. Moreover, the total potential energy is composed of bond angle bending potential energy, bond stretching potential energy, dihedral angle twisting potential energy, off-plane vibration potential energy, Waals potential energy and Coulomb electrostatic potential energy, shown in Equations (1).

$$E_{\text{potential}} = \sum_{\text{cross}} E(b,\theta,\varphi) + \sum_{\text{bond}} E_b(b) + \sum_{\text{torsion}} E_\varphi(\varphi) + \sum_{\text{angle}} E_\theta(\theta) + \sum_{\text{inversion}} E_x(x) + E_{ele} + E_{vdw} \tag{1}$$

where $E_{\text{potential}}$ is the total energy; $\sum_{\text{cross}} E(b,\theta,\varphi)$ represents the cross term potential energy; $\sum_{\text{bond}} E_b(b)$ is the bond stretching potential energy; $\sum_{\text{torsion}} E_\varphi(\varphi)$ is the dihedral angle twisting potential energy; $\sum_{\text{angle}} E_\theta(\theta)$ is the bond angle potential energy; $\sum_{\text{inversion}} E_x(x)$ is the off-plane vibration potential energy; E_{ele} is the Coulomb electrostatic potential energy and E_{vdw} is the Waals potential energy. The interaction between bitumen and corrosion products can be described by the 6/9 Lennard–Jones potential, as shown in Equations (2)-(3). The LJ 9-6 and Coulombic interactions are truncated to 10 Å and 8 Å.

$$E_{\text{ele}} = \sum_{i>j} \frac{q_i q_j}{r_{ij}} \tag{2}$$

$$E_{vdw} = \sum \boldsymbol{\varepsilon}_{ij} \left[2\left(\frac{r_{ij}^0}{r_{ij}}\right)^9 - 3\left(\frac{r_{ij}^0}{r_{ij}}\right)^6 \right] \tag{3}$$

where q_i and q_j are the charges of atomic i and j; r_{ij} is the distance of atomic i and j and $\boldsymbol{\varepsilon}_{ij}$ is the well depth of atomic i and j, respectively.

Each simulation consists primarily of the following steps: (1) Energy minimization was used to remove any potential energy excess that existed in the initial configuration. (2) The bio-rejuvenator/bitumen interface wetting model was then relaxed by NVT ensemble for 2 ns. 293 K, 333 K, 373 K, 408 K and 433 K were selected as the simulation temperature, which was corresponding to the original temperature, rutting temperature, induction heating temperature, paving temperature and mixing temperature. Simultaneously, the below 15 Å thickness of bitumen layer in each model was fixed in order to speed up calculation.

4 Results and Discussions

4.1 Phenomenon of dynamic wetting

In this MD simulation, the wettability of bio-rejuvenator nanodroplets on the bitumen surface of different simulated temperature with time were simulated. Figure 4 shows the snapshots of bio-rejuvenator nanodroplets on the bitumen at different simulated temperature with time in the wetting process. In the figure, the red parts represent the bio-rejuvenator nanodroplets and the blue part represent the bitumen. It can be found that the shape of nanodroplets weren't same with each other at different simulated temperature, which was caused by the reason that different temperatures were used in velocity initialization of the bio-rejuvenator nanodroplets. The nanodroplets with higher simulated temperature of velocity initialization would show large expansion and loose structure at 0 ns. During the dynamic spreading in the simulation, the nanodroplets would move to downward and get close to the bitumen surface firstly. When the nanodroplets got touch with bitumen, they would capture each other, and then the nanodroplets would extend dynamically on the surface of bitumen. However, the spreading rate of bio-rejuvenator nanodroplets on the bitumen were significantly different. It can also be found that the dynamic spreading of bio-rejuvenator nanodroplets on the bitumen would reach the equilibrium after 1.2 ns. The spreading of bio-rejuvenator nanodroplets would be faster and more flattened at high simulated temperature environment. Moreover, some molecules of bitumen and bio-rejuvenator nanodroplets would separate from the matrix, which wasn't shown in the Figure 4. It was caused by the large interaction and wouldn't affect the spreading process between bitumen and bio-rejuvenator nanodroplets. In the equilibrium stage, the contact angles of bio-rejuvenator nanodroplets with higher simulated temperature were less than that with lower simulated temperature, and they were all less than 90 degrees. It indicates that the spreading of bio-rejuvenator nanodroplets on the bitumen surface can happen spontaneously.

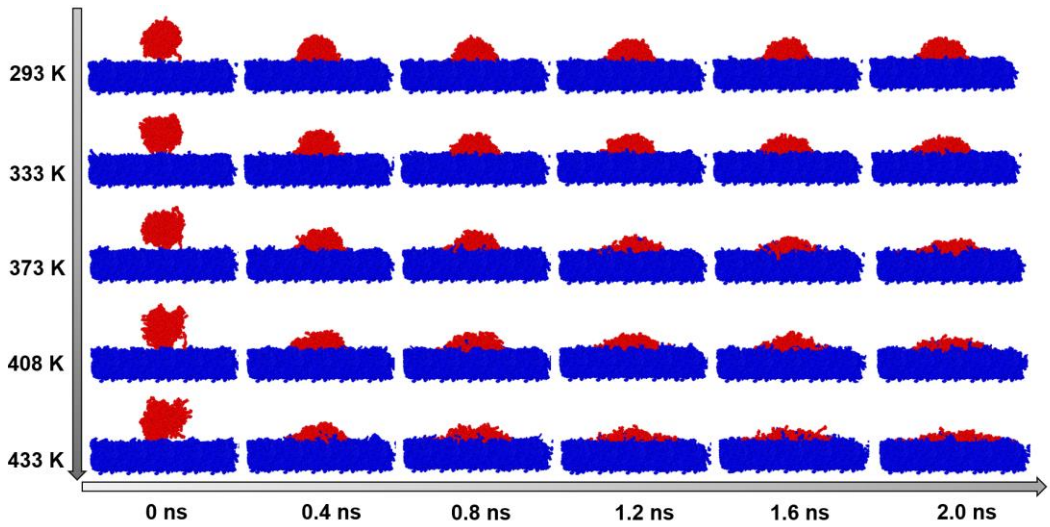

Figure 4. Wetting process of bio-rejuvenator nanodroplets on the bitumen at different temperature: Red (bio-rejuvenator nanodroplets), Blue (bitumen)

Trajectories of the bio-rejuvenator nanodroplets centroid were used to track the movement of the nanodroplets during the wetting process. Figure 5 shows the trajectories of the bio-rejuvenator nanodroplets centroid with simulated time in the Z coordinate. The trajectories of the bio-rejuvenator nanodroplets centroid at different simulated temperature were similar to each other. The curves can be divided into three stages: Rapidly descent stage, slowly descent stage and dynamic equilibrium stage. It can be found that the bio-rejuvenator nanodroplets would get close to the surface of bitumen rapidly while the stage would last for a very short time compared with the whole simulation, and the time was around 100 ps. Then slowly descent stage was followed when the velocity of descent would decease gradually with time until it reached a relatively fixed value. The time would last for a long time which was around 1 ns. The final was dynamic equilibrium stage where the bio-rejuvenator nanodroplets would either continue to descent at a very slow velocity or fluctuate slowly, which was related to the simulated temperature. It can be found that the velocity of bio-rejuvenator nanodroplets at high temperature (373 K, 408 K and 433 K) was similar to that at low temperature (293 K and 333 K) at rapidly descent stage but obviously larger than that at slowly descent stage. It was consistent with the more flattened shape of bio-rejuvenator nanodroplets at high temperature. Moreover, the centroid position of bio-rejuvenator nanodroplets at high temperature at dynamic equilibrium stage was found unstable. It was caused by the reason that the bitumen and bio-rejuvenator nanodroplets in the temperatures had reached the flowing statement which would intensify the dynamic spreading. Especially bio-rejuvenator nanodroplets at 433 K has the most violent fluctuations and there was even a tendency to continue to spread rapidly.

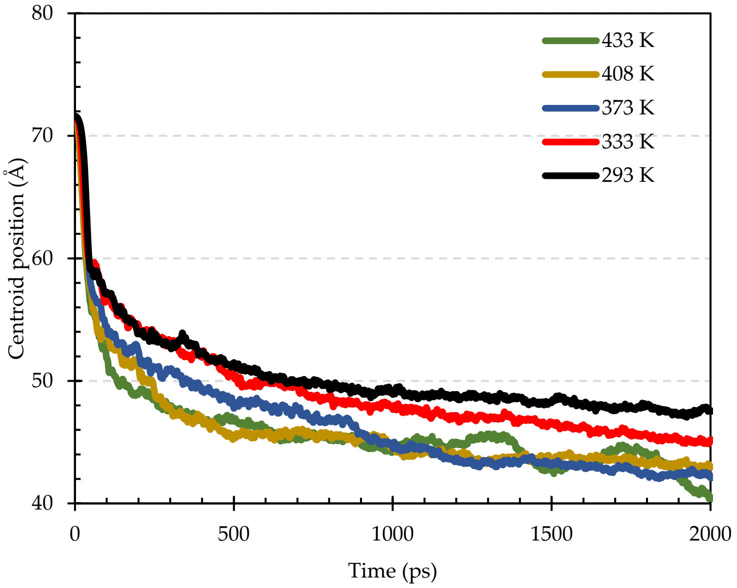

Figure 5. Trajectories of the bio-rejuvenator nanodroplets centroid with simulated time

Total energy (sum of kinetic energy and potential energy) of bio-rejuvenator nanodroplets/bitumen interface wetting model changing with simulated time was obtained to quantify the energy changing of the system during the wetting process. The convergence of total energies of bio-rejuvenator nanodroplets/bitumen interface wetting model with simulated time is shown in the Figure 6. The initial total energy of the models were different due to the different temperature used in velocity initialization. After a geometry optimization process, the bio-rejuvenator nanodroplets/bitumen interface wetting model can achieve the energy equilibrium with the dynamics equilibration with NVT ensemble for 500 ps. The extra 1.5 ns simulation with NVT ensemble can be used for the subsequent trajectory analysis and calculations. It is clearly that the total energy of the systems was all increased when simulated temperature was raised. It was supported by the increment of potential energy and kinetic energy individually. This is mostly due to the fact that the heat energy in the system is constantly transformed into internal energy as the temperature rises, increasing the internal energy. The kinetic energy of the systems was similar and would be increased gradually by the increased temperature, which was related to the intensified irregular movements of molecules in the system. Moreover, the energy fluctuation of the system at high temperature was obviously severe, which was also influenced by the intensified irregular movements of molecules. It can also be observed that the time of the models to reach the equilibrium state was similar, but higher temperature would still make the time slightly shorter. Difference between initial value and equilibrium value of total energy would incease with the increment of temperature. It indicates that the models at high temperature should be more difficult to achieve equilibrium theoretically, but its equilibrium efficiency was higher in fact. Furthermore, it can be also concluded that the equilibrium of energy cannot fully represent the equilibrium of molecular movement. After the total energy has reached the equilibrium around 500 ps, the molecular movement of bio-rejuvenator nanodroplets and bitumen were still severe, which led to the continuous downtrend movement of bio-rejuvenator nanodroplets and the changing of contact angle.

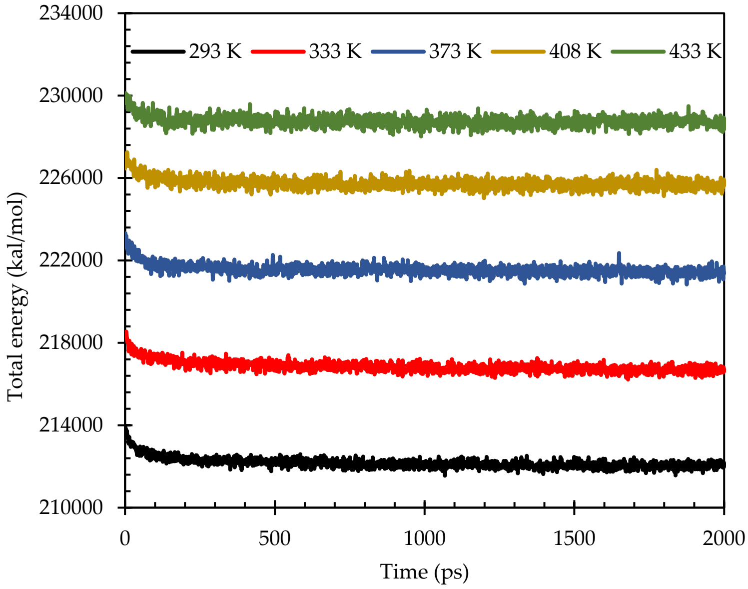

Figure 6. The convergence of total energies of bio-rejuvenator nanodroplets/bitumen interface wetting model with simulated time

4.2 Analysis of contact angles

The changes in the morphology and spreading behaviors of bio-rejuvenator nanodroplets reflect variances in wettability, which was analyzed by the calculation of contact angle based on the bio-rejuvenator nanodroplets shape. The contours can be obtained from the frame by circular fitting of the profiles through the least square method, and the circle can be fitted by Equation (5) and the contact angle can be calculated by Equation (6) and (7). Frames within $\pm$ 10 ps at the selected time point with the interval of 1 ps were used to obtain the contact angle to ensure the accuracy of measurement.

$$(x-a)^2+(z-b)^2=\mathrm{R}^2 \tag{5}$$

$$\theta ti=\arccos\left(\frac{\mathrm{R}-b}{R}\right) \tag{6}$$

$$\theta=\sum\nolimits_{t-10}^{t+10}\theta ti \tag{7}$$

Where a and b are the X and Z coordinates of the fitted circle's center point, respectively. R is the radius of fitting circular. θti is the contact angle of ti ps. t is the selected time point. θ is the average value of contact angle within $\pm$ 10 ps at selected time points, which would be shown in Figure 7.

Figure 7 show the contact angle between bio-rejuvenator nanodroplets and bitumen in different temperature with time changing. Similar to Figure 5, the curves of contact angles can also be divided into three stages shown in Figure 7 (a): Rapidly descent stage, slowly descent stage and dynamic equilibrium stage. It can be found that contact angles would decrease rapidly for a short time firstly, which was corresponding to the rapid decent of bio-rejuvenator nanodroplets. Then the decent velocity would decrease gradually until it reached around a stable value. It was clearly that higher temperature would make bio-rejuvenator nanodroplets present a smaller contact angle on the surface of bitumen, indicating the better wettability in high temperature environment. Moreover, it can be obversed that there is a tendency to continue to decrease of contact angles of bio-rejuvenator nanodroplets, especially of the lower temperature. Figure 7 (b) illustrates the changing of equilibrium contact angle with different simulated temperature. It can be found that the contact angles would increase linearly with the increment of temperature, and the coefficient of determination R^2 of 0.9972 indicates the nice fitting effect of the linear model, which can be used to predict the contact angle at other temperature.

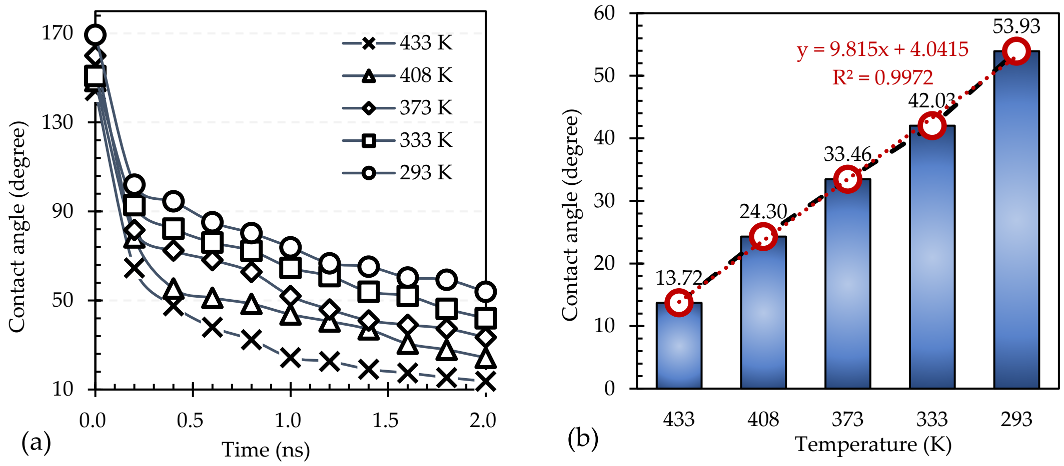

Figure 7. Contact angle between bio-rejuvenator nanodroplets and bitumen: (a) Changing of contact angle with simulated time; (b) Changing of equilibrium contact angle with different simulated temperature.

Figure 8 shows the wetting statement of bio-rejuvenator nanodroplets on the bitumen. The contact angle can be used as the index to determine the wetting statement: 1) When θ=0 degree , it is completely wetting; 2) when θ < 90 degree, it is partially wetting; 3) When θ = 90 degree, it is the dividing line of wetting or not; 4) When θ > 90 degree, it will not wetting; 5) When θ = 180 degree, it is completely non-wetting. With increasing time, the interaction between bio-rejuvenator nanodroplets and bitumen would be enhanced, leading to a shift from non-wetting to partial wetting. The interval time of nonwetting and partial wetting was distinct of bio-rejuvenator nanodroplets at different temperature. It was 0.12 ns, 0.15 ns, 0.16 ns, 0.23 ns and 0.51 ns corresponding to 433 K, 408 K, 373 K, 333 K and 293 K respectively, which indicates that high temperature makes the transition of nonwetting and partial wetting more rapidly. It can be found that the bio-rejuvenator nanodroplets at 433 K has nearly spreaded completely with a contact angle of 0° when simulated time kept going on, but it still can’t reach the complete wetting statement. Therefore, unlimited increment of temperature had little significance to the wetting of bio-rejuvenator nanodroplets on bitumen. Conversely, extending time appropriately may be more beneficial to wetting process.

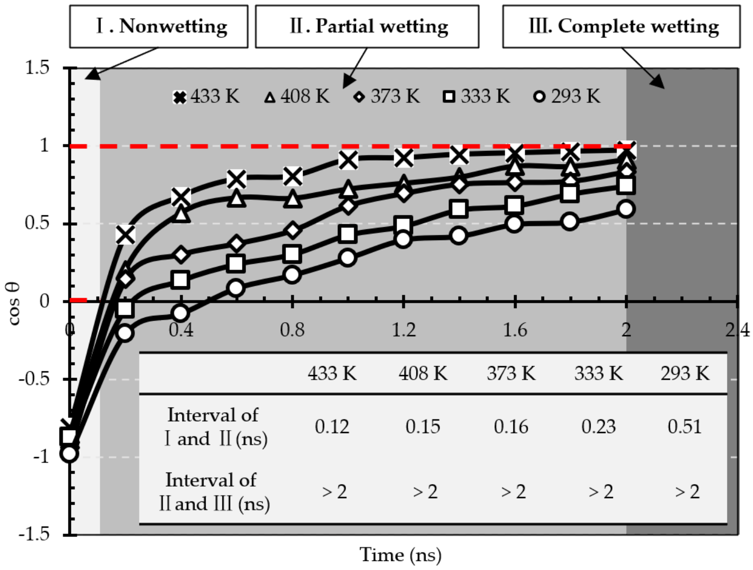

Figure 8. Wetting statement of bio-rejuvenator nanodroplets on the bitumen by contact angles

4.3 Wetting dynamics movement of nanodroplets

In the wetting process, the shape of bio-rejuvenator nanodroplets would keep the circular arc firstly and then some molecules of bio-rejuvenator nanodroplets preferentially form a layer of film on the bitumen surface, which is called precursor film. To gain insight of this phenomenon, the number density profiles of bio-rejuvenator nanodroplets atoms of X-Z plane were calculated. Figure 9 (a)-(e) shows the atom number density profiles of bio-rejuvenator nanodroplets on bitumen at different simulated temperatures. The white parts are the main section of bio-rejuvenator nanodroplets, and the red parts are the precursor film of bio-rejuvenator nanodroplets. The generation of precursor film is caused by the fact that surface of bio-rejuvenator nanodroplets molecules are more unstable and active than the inside one due to unsaturated electrostatic and hydrogen bond interactions. As a result of the strong attraction between the bio-rejuvenator nanodroplets and the bitumen surface, preferential adsorption would occur and result in the creation of a precursor film. Precursor film is actually the thin and limited-thickness film that propagates in front of the droplet contact line and governs wetting behavior, which has been confirmed in numerous researches (A et al., 2020; Benhassine et al., 2011). It was discovered that as time passed, molecules of bio-rejuvenator nanodroplets gradually spreaded to both sides after the contact with bitumen, while the peak value of the maximum concentration gradually dropped. The molecules in the main section of bio-rejuvenator nanodroplets would gradually enter the precursor film and become apart of it, which led to the forward moving of precursor film and the increment of thickness of precursor film. As shown in Figure 9 (f), changing of atom number density of precursor film of bio-rejuvenator nanodroplets with different simulated temperatures can be described as the liner relationship. There were more molecules in the precursor film of the models at high temperature. It also can be observed that the diffusion range of the models at high temperature would stop changing faster.

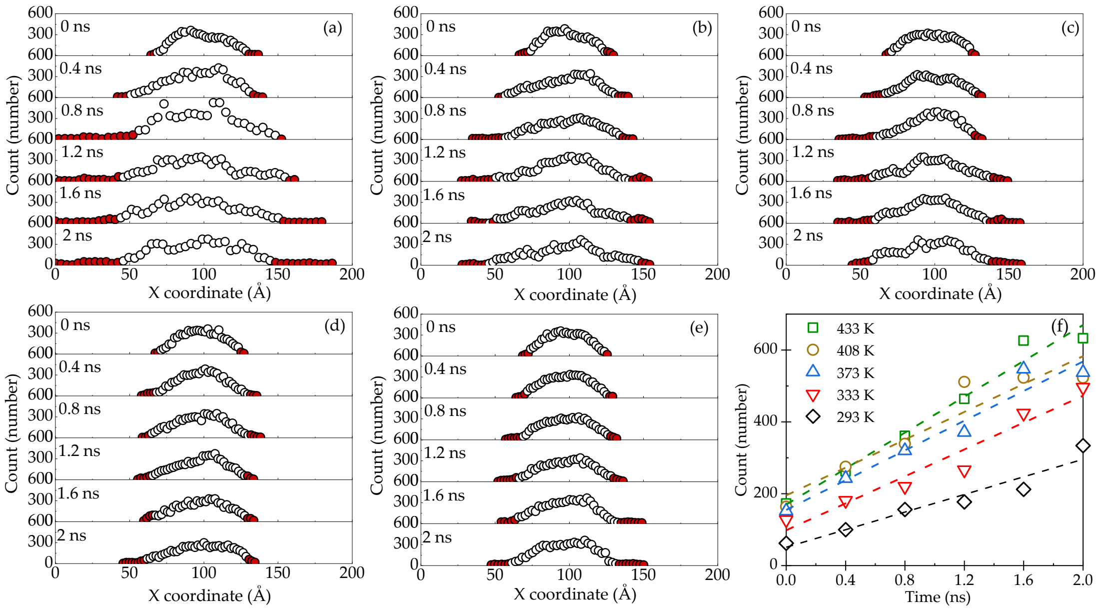

Figure 9. (a)-(e) Atom number density profiles of bio-rejuvenator nanodroplets on bitumen at different simulated temperatures: (a) 293 K, (b) 333K, (c) 373 K, (d) 408 K and (e) 433 K. (f) Atom number density of precursor film of bio-rejuvenator nanodroplets at different simulated temperatures

The contact line velocity was also be investigated in this research, which would be obtained from the relationship of simulated time and $R \times \sin\theta$ in Equation (5). Commonly, it would be fitted by a set of ratios of polynomials in the form of $R = \frac{p_0+p_1 t+p_2 t^2+\ldots+p_n t^n}{1+p_1' t+p_2' t^2+\ldots+p_n' t^n}$). The polynomial order is varied and the best fit was used in this research of the presented simulations, where an order n = 2 was successfully. The best fit is determined by the consecutive use of a downhill simplex method starting with a randomly distributed initial parameter and a Levenberg Marquardt algorithm with the fitted simplex parameters as starting points. Then, the contact line speed can be obtained by deriving the fitting formula above. Figure 10 shows the relationship between the contact line velocity (V) and contact angle at different simulated temperature. With the change of time, the trend of contact line velocity decreasing gradually can be observed. The decrement was different from the previous studied about wetting where the commonly used Molecular-Kinetic Theory (MKT) linear model was used to describe the relationship. It can be found that contact line velocity of the models at 293 K, 333 K and 373 K were changing with time linearly, while that at 408 K and 433 K first non-linearly decreased and then linearly decreased. At the beginning of wetting, the bio-rejuvenator nanodroplets and bitumen were still catching each other, which was greatly influenced by the temperature. Moreover, the bio-rejuvenator nanodroplets at high temperature possessed faster contact line velocity while its decrement was so obviously. The results also indicate that the bio-rejuvenator nanodroplets had larger contact line velocity, as well as the larger decrement rate of contact line velocity.

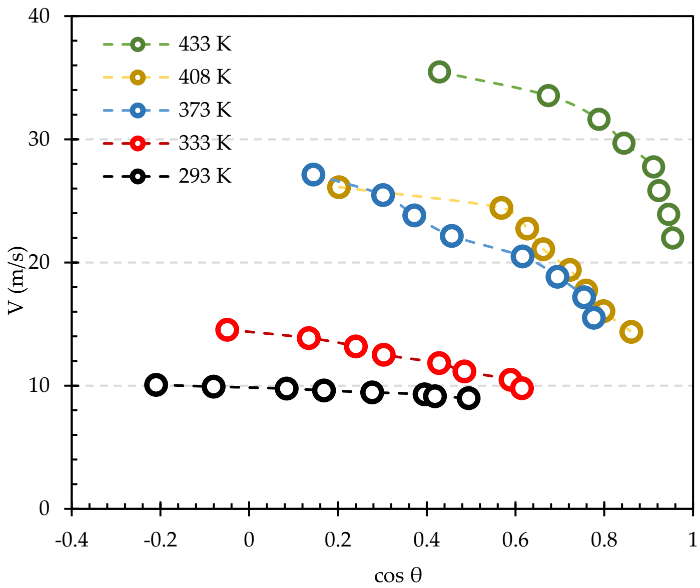

Figure 10. Relationship between the contact line velocity (V) and contact angle at different simulated temperature

4.4 Interaction effect

Figure 11 shows MSD curves and diffusion coefficients of bio-rejuvenator nanodroplets/bitumen interface wetting model. Mean squared displacement (MSD) was used to investigate the molecules movement of bio-rejuvenator nanodroplets on the bitumen over simulated time. The core regulation of diffusion phenomena was the movements of atoms in three-dimension space, which was vital to analyze the interaction between bitumen and corrosion products. However, due to the enormous number of atoms in the interface system, detecting each atom's motion trajectory is difficult. As a result, mathematical statistics method was held to describe the regularity of particle movement. The most commonly used indicator was mean square displacement (MSD), which would be represented and calculated by Equation (1):

$$\mathrm{MSD}(t) = \langle |r_i(t) - r_i(0)|^2 \rangle \tag{1}$$

Where, $\mathrm{MSD}(t)$ indicated as the mean value of all atoms' movement positions in the molecular system, $r_i(0)$ indicated the original position of particle i, and $r_i(t)$ indicated the position of particle i at the time of t.

It is clearly that the MSD curves can be divided into two stages (rapid rising period and linear rising period). The rapid rising period would last for a short time and then linear rising period was followed which can be used to calculate the diffusion coefficient. The MSD calculation was based on simple diffusion mode (Brownian motion), during which MSD was a quadratic function of correlation time in the initial short time, representing barrier-free directional diffusion. With the increase of correlation time, MSD will quickly transform to a linear function stage, which represents normal diffusion. This linear function region is generally the best region for calculating diffusion coefficient. It can be found that the rapid rising period was relatively short while the linear rising period was longer. Meanwhile the fluctuation of MSD curves would be more severe at high temperature, which indicates that the movement of bio-rejuvenator nanodroplets in systems would be increased by the higher temperature.

Diffusion coefficient, for the measurement of the molecule's capacity for diffusion, rate at which a quantity diffuses per unit area while the concentration gradient is the same unit. MSD had a linear relationship with time and was correlated with the diffusion coefficient after diffusion relaxation process. After this period, the linear slope of the MSD curve might be used to compute the diffusion coefficient of the contact system, as indicated by Equation (2):

$$D = \frac{1}{6N} \lim_{t\to\infty} \frac{d}{dt} \sum_{i=1}^{N} \langle |r_i(t) - r_i(0)|^2 \rangle \tag{2}$$

Where, the diffusion coefficient was recorded as D in the interface system, N indicated the whole number of molecules in the interface system, and the differential term was equal to the linear slope of the interface system's MSD curve.

Equation (2) showed that there was a linear relationship between the diffusion coefficient and the slope of the MSD curve. Nevertheless, Equation (2) ignored the actual simulation scenario and was expressed in an ideal condition of indefinite period. As a result, Equation (3) illustrates how the diffusion coefficient calculation formula was really approximated in the calculation:

$$D \approx \frac{1}{6} K_{MSD} \tag{3}$$

Where K_{MSD} was equal to the linear slope of the interface system's MSD curve.

It is necessary to determine the simulated time range used for the fitting to calculate the diffusion coefficient. In this research, the MSD curves was transformed into double logarithmic form (log(MSD)-log(t)), then select a section whose slope is as close to 1 as possible to find the diffusion coefficient. Base on Equation (3), and it would be as follows:

$$\log \mathrm{MSD}(t) = \log t + \log(6D) \tag{4}$$

Where MSD is mean squared displacement, t is the simulated time and D is diffusion coefficient.

By this method, the diffusion coefficients of bitumen-corrosion products system at different temperatures were calculated and shown in Figure 11. A higher slope of MSD curves means a greater diffusivity of molecules. It is found that bio-rejuvenator nanodroplets on bitumen surface under different temperature possessed distinct diffusion coefficient. The diffusion coefficients of bio-rejuvenator nanodroplets/bitumen interface wetting model with different temperature basically showed the regularity of 433 K > 408 K > 373 K > 333 K > 293 K. The results showed that the diffusivity of bio-rejuvenator nanodroplets on the surfaces of bitumen was positively correlated with simulated temperature. It would be caused by the contribution both of bio-rejuvenator nanodroplets and bitumen. The increase of temperature led to the decrement of viscosity of bio-rejuvenator nanodroplets and bitumen. bio-rejuvenator is a liquid itself, and there is the limitation for the decrement of its viscosity. Under this limitation, the viscosity of bitumen can continue to decrease rapidly, so that the diffusion coefficient continued to increase.

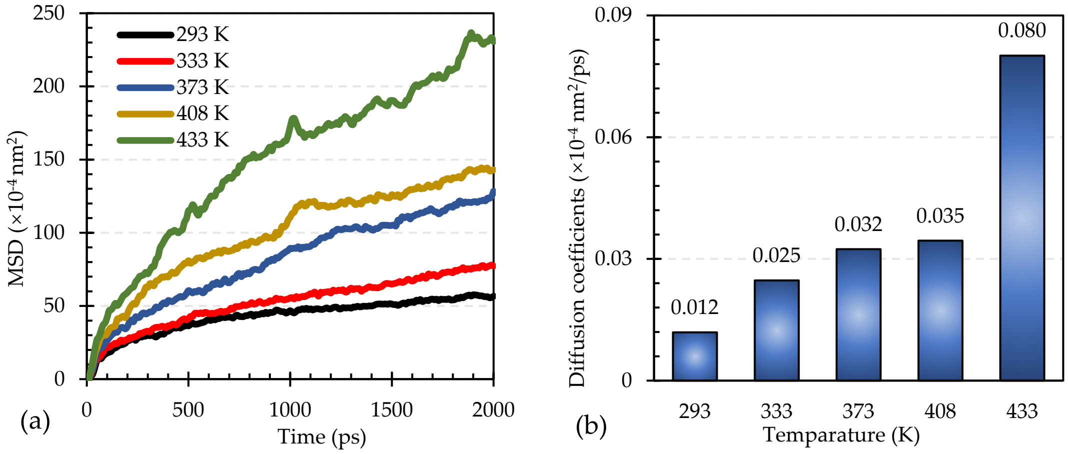

Figure 11. The quantification of diffusion in bio-rejuvenator nanodroplets/bitumen interface wetting model: (a) MSD curves; (b) Diffusion coefficients

Interaction energy (E_{inter}) could be used to evaluate the stability of interface of bitumen and bio-rejuvenator nanodroplets. Adhesion work ($W_{adhesion}$) could be used to stand for the interfacial bonding strength of bitumen and bio-rejuvenator nanodroplets. The greater the absolute value of E_{inter} and $W_{adhesion}$, the more interaction there was between bitumen and bio-rejuvenator nanodroplets. When the value of E_{inter} was zero or positive, adsorption was minor or non-existent. Their calculation formula was shown in Equation (4)-(5).

$$E_{inter} = E_{bitumen} + E_{bio-rejuvenator\ nanodroplets} - E_{total} \tag{4}$$

$$W_{adhesion} = \frac{E_{inter}}{A} \tag{5}$$

Where E_{inter} represented the interaction energy between bitumen and bio-rejuvenator nanodroplets, $W_{adhesion}$ represented the adhesion work between bitumen and bio-rejuvenator nanodroplets, E_{total} represented that the total potential energy of the bitumen- bio-rejuvenator nanodroplets system in a steady state, $E_{bitumen}$ represented the total potential energy of bitumen, $E_{bio-rejuvenator\ nanodroplets}$ represented the total potential energy of bio-rejuvenator nanodroplets. A represented the contact area of bitumen and bio-rejuvenator nanodroplets, which was approximate as a circular and its radius was equal to the R in equation (5).

Figure 12 presents the interaction effect between bio-rejuvenator nanodroplets and bitumen including interaction energy and adhesion work respectively. It can be found that the interaction energy would increase gradually with the simulated time kept going. In the increasing period, the increasing velocity of interaction energy was followed as: 433 K > 408K > 373 K > 333 K > 293 K, while it was similar for the models at 373 K, 408 K and 433 K, as well as the models at 293 K and 333 K in the equilibrium period. The interaction energy of the models at 373 K, 408 K and 433 K were significantly larger than that at 293 K and 333 K. Figure 12 (b) show the changing of adhesion work between bio-rejuvenator nanodroplets and bitumen with the simulated temperature. The $W_{adhesion}$ would firstly increases rapidly, reach the peak and then decrease. The peak of $W_{adhesion}$ occurs in the models at 373 K, which indicated that the wettability would be the worse due to that the maximum energy was needed to separate bio-rejuvenator nanodroplets from bitumen.

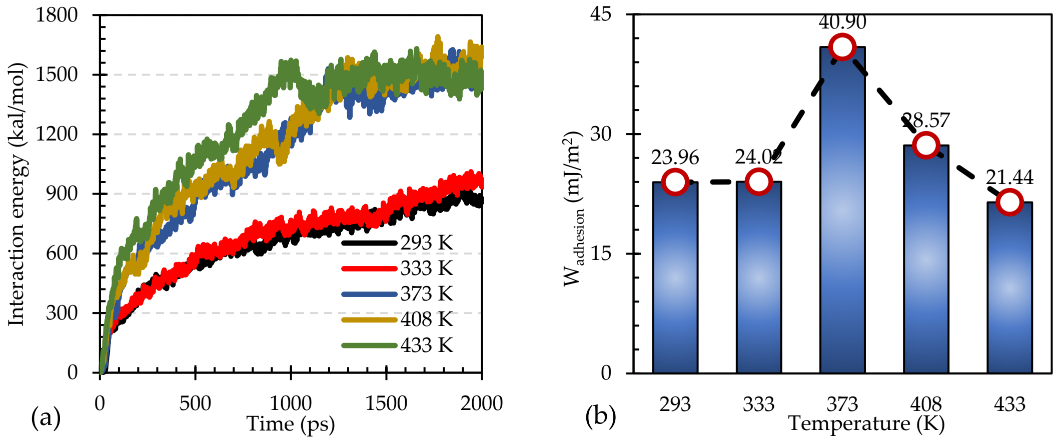

Figure 12. The interaction effect between bio-rejuvenator nanodroplets and bitumen with simulated time: (a) Interaction energy; (b) Adhesion work

Contact angle can also be used for the calculation of adhesion work, as well as infiltration work. The relationship between the contact angle and adhesion work, infiltration work is shown in the Equations (6) and (7).

$$W_a = \gamma_V(\cos(\theta) + 1) \quad (6)$$

$$W_i = \gamma_V cos(\theta) \quad (7)$$

Where W_a is the adhesion work calculated by contact angle, W_i is the infiltration work calculated by contact angle, γ_V is the surface tension at different temperature obtained from the previous researches.

Figure 13 shows the W_a and W_i of the bio-rejuvenator nanodroplets on bitumen at different temperatures. W_i would increase rapidly before the peak value occcured, and then it would fluctuate dynamiclly. The result indicates that bio-rejuvenator nanodroplets and bitumen would infiltrate each other with the increment of temperature. However, there was a limitation for the infiltration degree. It can be also found that W_a presented the similar trend with different temperature with $W_{adhesion}$, meanwhile W_a and $W_{adhesion}$ had the same order of magnitude. The difference might be caused by the approximate calculation of contact area between bio-rejuvenator nanodroplets on bitumen. Therefore, it can be concluded that the increasing diffusion degree of bio-rejuvenator nanodroplets and bitumen with temperature in the practical engineering was contributed by the combination of wetting and infiltration before 373 K. After 373 K, the increment was supported by wetting mainly. Furthermore, the suggestion temperature for the combination of induction heating technology and encapsulation technology should avoid the value around 373 K, which would be beneficial for the diffusion of bio-rejuvenator nanodroplets on bitumen. The suggestion depends on the determination of rejuvenator type in the encapsulation.

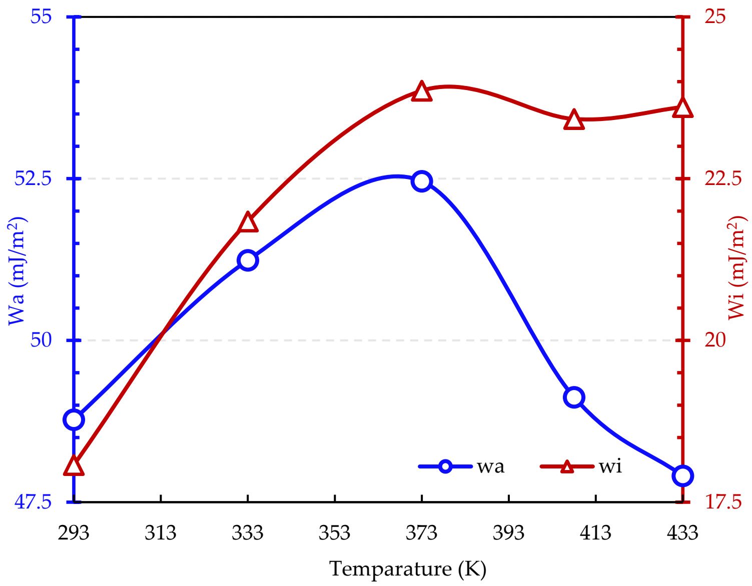

Figure 13. W_a and W_i of the bio-rejuvenator nanodroplets on bitumen at different simulated temperatures

4.5 Hysteresis of contact angle

In the wetting process, the bio-rejuvenator nanodroplets would be affected by the external force to chang the wetting statement. So, hysteresis of contact angle was also investigated in research. After the bio-rejuvenator nanodroplets have reached the equilibrium state, the external force in the positive direction of x axis of 0.05 kal/mol/ Å and 0.1 kal/mol/ Å were applied to the nanodroplets respectively. Figure 14 shows the contact angle hysteresis of bio-rejuvenator nanodroplets on bitumen surface at different temperature and different external force. It can be found that when an external force in the X direction was applied to the bio-rejuvenator nanodroplets, it will be deformed and form a forward angle θ_A and a backward angle θ_B. The difference of θ_A and θ_B is the hysteresis of contact angle, which was defined as $\Delta\theta$.

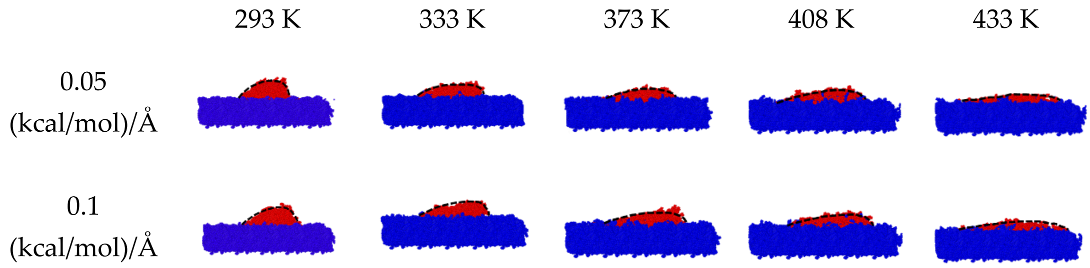

Figure 14. Contact angle hysteresis of bio-rejuvenator nanodroplets on bitumen surface

Figure 15 shows the quantification of contact angle hysteresis of bio-rejuvenator nanodroplets on bitumen surface. It can be found that the forward angle was always larger than the backward angle, meanwhile the forward angle and backward angle of bio-rejuvenator nanodroplets by 0.05 (kcal/mol)/Å were larger than that by 0.1 (kcal/mol)/Å. This was caused by the reason that when the external force was small, it was difficult to push the part where the bio-rejuvenator nanodroplets contacted the bitumen, which would lead to severe hysteresis. It can also be proved by the value of $\Delta\theta$, which of bio-rejuvenator nanodroplets by 0.1 (kcal/mol)/Å was obviously less than that by 0.05 (kcal/mol)/Å. Furthermore, the increasing temperature would weaken the hysteresis of contact angle.

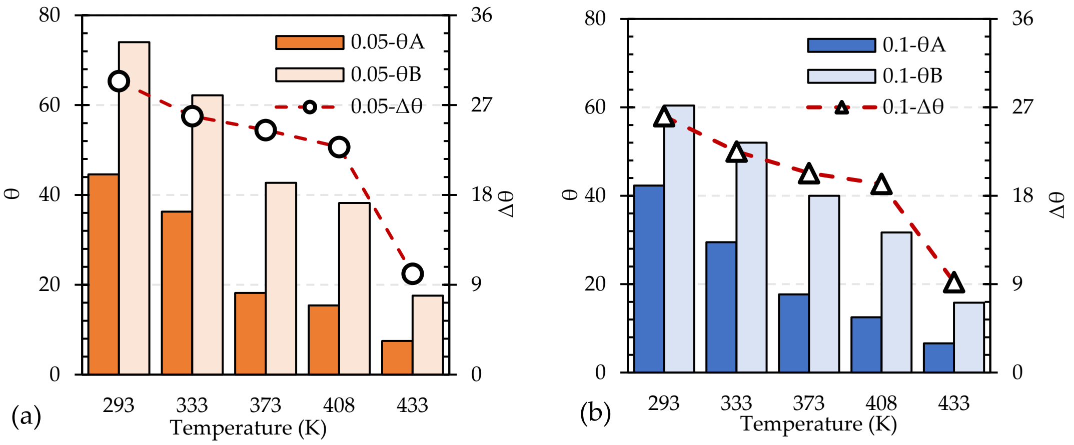

Figure 15. Quantification of contact angle hysteresis of bio-rejuvenator nanodroplets on bitumen surface: (a) External force of 0.05 (kcal/mol)/Å; (b) External force of 0.1 (kcal/mol)/Å

5 Conclusions

The investigation has been carried out to identify wetting process of bio-rejuvenator nanodroplets on bitumen at different temperatures by molecular dynamics simulation approach. Based on the results, the primary conclusions are as follows:

(1) In the wetting process, the bio-rejuvenator nanodroplets will first approach the bitumen quickly, and then slow down to an equilibrium state. There is no consistency between the energy equilibrium of the bio-rejuvenator nanodroplets/bitumen interface wetting model and the movement equilibrium of bio-rejuvenator nanodroplets, where a delay of about 1ns existed between them.

(2) The contact angle of bio-rejuvenator nanodroplets will gradually decrease with the extension of time. The equilibrium contact angle of nanodroplets varies linearly with simulated temperature. The time for the nanodroplets reaching partial-wetting state decreases with the increment of temperature, but it is difficult to reach complete-wetting state, even the temperature has reached 433 K.

(3) The precursor film of the bio-rejuvenator nanodroplets will spread first in the wetting process, and the molecules in the nanodroplets will gradually enter the precursor film until an equilibrium state was reached. The relationship between contact linear velocity and cosine of contact angle is linear after nanodroplets and bitumen had caught each other.

(4) High temperature is beneficial to the diffusion of bio-rejuvenator nanodroplets on bitumen. Increasing mixing degree of bio-rejuvenator nanodroplets and bitumen with the increase of temperature was contributed by the combination of wetting and infiltration before 373 K, after which the increment was supported by wetting mainly.

(5) The application of external force will cause hysteresis of bio-rejuvenator nanodroplets. When the external force was small, it was difficult to push the part where the bio-rejuvenator nanodroplets contacted the bitumen, which would lead to severe hysteresis. The higher temperature can weaken the hysteresis of contact angle. More research on nanodroplet size, temperature and force should be carried out in the future.

This study exploits molecular dynamics to visualize the wetting process and explores the wetting characteristics of the bio-rejuvenator nanodroplets on bitumen. These findings are contributed to the utilization of rejuvenators in the pavement engineering. Meanwhile, it can be considered to determine the time of wetting and diffusion to adopt different temperatures. Furthermore, more rejuvenators can be also considered in the future.

Author Contributions: **Haiqin Xu**: Conceptualization, Methodology, Data curation, Writing-Original draft, Writing - Review & Editing. **Yingxue Zou**: Methodology, Data curation, Writing - Review & Editing. **Gordon Airey**: Investigation, Writing - Review & Editing. **Haopeng Wang**: Methodology, Investigation, Data curation. **Hanyu Zhang**: Methodology, Investigation, Data curation. **Shaopeng Wu**: Conceptualization, Funding acquisition, Supervision. **Anqi Chen**: Conceptualization, Methodology, Project administration.

Acknowledgement: This research was supported by the National Natural Science Foundation of China (No.52378461 and No. 52208444), Key R&D Program of Guangxi Province (No. AB21196061), Hubei Science and Technology Innovation Talent and Service Project (International Science and Technology Cooperation) (2022EHB006) and Science and Technology Project of the Department of Transportation of Guangxi Autonomous Region (2021-MS5-125). This study was also supported by Program of China Scholarships Council (No. 202206950033). Finally, we are grateful for access to the University of Nottingham's Augusta HPC service.

Declaration of Competing Interest: The authors declare that they have no known competing financial interests or personal relationships that could have appeared to influence the work reported in this paper.

Reference

A, H., Yang, Z., Hu, R., Chen, Y.-F., Yang, L., 2020. Effect of Solid–Liquid Interactions on Substrate Wettability and Dynamic Spreading of Nanodroplets: A Molecular Dynamics Study. J. Phys. Chem. C 124, 23260–23269. https://doi.org/10.1021/acs.jpcc.0c07919

Benhassine, M., Saiz, E., Tomsia, A.P., De Coninck, J., 2011. Nonreactive wetting kinetics of binary alloys: A molecular dynamics study. Acta Mater. 59, 1087–1094. https://doi.org/10.1016/j.actamat.2010.10.039

Cao, Z., Chen, M., Yu, J., Han, X., 2020. Preparation and characterization of active rejuvenated SBS modified bitumen for the sustainable development of high-grade asphalt pavement. J. Clean. Prod. 273. https://doi.org/10.1016/j.jclepro.2020.123012

Cui, P., Wu, S., Xiao, Y., Hu, R., Yang, T., 2021. Environmental performance and functional analysis of chip seals with recycled basic oxygen furnace slag as aggregate. J. Hazard. Mater. 405, 124441. https://doi.org/10.1016/j.jhazmat.2020.124441

Cui, P., Wu, S., Xu, H., Lv, Y., 2019. Silicone Resin Polymer Used in Preventive Maintenance of Asphalt Mixture Based on Fog Seal. Polym. Basel 11. https://doi.org/10.3390/polym11111814

Ding, Y., Li, D., Wang, Y., Wei, W., 2022. Prediction of the Rejuvenator Diffusion Coefficient in Aged Asphalt Based on Free Volume Theory. ACS Sustain. Chem. Eng. https://doi.org/10.1021/acssuschemeng.2c06215

European Commission. Directorate General for Regional and Urban Policy., 2022. Road infrastructure in Europe: road length and its impact on road performance. Publications Office, LU.

European Union Road Federation (ERF), 2014. Road Asset Management: An ERF Position Paper for Maintaining and Improving a Sustainable and Efficient Road Network.

Fang, Y., Zhang, Z., Zhang, H., Li, W., 2022. Analysis of wetting behavior and its influencing factors of rejuvenator/old asphalt interface based on surface wetting theory. Constr. Build. Mater. 314. https://doi.org/10.1016/j.conbuildmat.2021.125674

Hu, Y., Si, W., Kang, X., Xue, Y., Wang, H., Parry, T., Airey, G.D., 2022. State of the art: Multiscale evaluation of bitumen ageing behaviour. FUEL 326. https://doi.org/10.1016/j.fuel.2022.125045

Jennings, P.W., National Research Council, 1993. Binder characterization and evaluation by nuclear magnetic resonance spectroscopy, Strategic Highway Research Program, SHRP-A. Washington, DC.

Karlsson, R., Isacsson, U., 2003. Application of FTIR-ATR to characterization of bitumen rejuvenator diffusion. J. Mater. Civ. Eng. 15, 157–165. https://doi.org/10.1061/(ASCE)0899-1561(2003)15:2(157)

Karlsson, R., Isacsson, U., Ekblad, J., 2007. Rheological characterisation of bitumen diffusion. J. Mater. Sci. 42, 101–108. https://doi.org/10.1007/s10853-006-1047-y

Li, D.D., Greenfield, M.L., 2014. Chemical compositions of improved model asphalt systems for molecular simulations. Fuel 115, 347–356. https://doi.org/10.1016/j.fuel.2013.07.012

Li Haibin, Yang Fayong, Zhang Fan, Zou Xiaolong, Zhao Guijuan, 2021. Diffusion and Regeneration Mechanism of Waste Composite Oils Rejuvenator in Aged Asphalt. J. WUHAN Univ. Technol.-Mater. Sci. Ed. 36, 664–671. https://doi.org/10.1007/s11595-021-2458-y

Li, Y., Li, H., Nie, S., Wu, S., Liu, Q., Li, Chuangmin, Shu, B., Li, Chao, Song, W., zou, Y., Pang, L., 2020. Negative impacts of environmental factors (UV radiation, water and different solutions) on bitumen and its mechanism. Constr. Build. Mater. 265. https://doi.org/10.1016/j.conbuildmat.2020.120288

Ministry of Transport of the People's Republic of China, 2023. Statistical Bulletin on the Development of Transportation Industry in 2022 [WWW Document]. URL https://xxgk.mot.gov.cn/2020/jigou/zhghs/202306/t20230615_3847023.html (accessed 6.17.23).

Rathore, M., Haritonovs, V., Meri, R.M., Zaumanis, M., 2022. Rheological and chemical evaluation of aging in 100% reclaimed asphalt mixtures containing rejuvenators. Constr. Build. Mater. 318. https://doi.org/10.1016/j.conbuildmat.2021.126026

Shu, B., Wu, S., Dong, L., Norambuena-Contreras, J., Li, Y., Li, C., Yang, X., Liu, Q., Wang, Q., Wang, F., Barbieri, D.M., Yuan, M., Bao, S., Zhou, M., Zeng, G., 2020. Self-healing capability of asphalt mixture containing polymeric composite fibers under acid and saline-alkali water solutions. J. Clean. Prod. 268. https://doi.org/10.1016/j.jclepro.2020.122387

Su, J., Wang, Y., Yang, P., Han, S., Han, N., Li, W., 2016. Evaluating and Modeling the Internal Diffusion Behaviors of Microencapsulated Rejuvenator in Aged Bitumen by FTIR-ATR Tests. MATERIALS 9. https://doi.org/10.3390/ma9110932

Tabaković, A., Faloon, C., O'Prey, D., 2022. The Effect of Conductive Alginate Capsules Encapsulating Rejuvenator (HealRoad Capsules) on the Healing Properties of 10 mm Stone Mastic Asphalt Mix. Appl. Sci. 12, 3648. https://doi.org/10.3390/app12073648

Tian, T., Jiang, Y., Fan, J., Yi, Y., Deng, C., 2021. Development and Performance Evaluation of a High-Permeability and High-Bonding Fog-Sealing Adhesive Material. MATERIALS 14. https://doi.org/10.3390/ma14133599

Wan, P., Liu, Q., Wu, S., Zhao, Z., Chen, S., Zou, Y., Rao, W., Yu, X., 2021. A novel microwave induced oil release pattern of calcium alginate/ nano-Fe3O4 composite capsules for asphalt self-healing. J. Clean. Prod. 297. https://doi.org/10.1016/j.jclepro.2021.126721

Wan, P., Liu, Q., Wu, S., Zou, Y., Zhao, F., Wang, H., Niu, Y., Ye, Q., 2022. Dual responsive self-healing system based on calcium alginate/Fe3O4 capsules for asphalt mixtures. Constr. Build. Mater. 360. https://doi.org/10.1016/j.conbuildmat.2022.129585

Wang, J., Li, Q., Lu, Y., Luo, S., 2022. Effect of Waste-Oil regenerant on diffusion and fusion behaviors of asphalt recycling using molecular dynamics simulation. Constr. Build. Mater. 343. https://doi.org/10.1016/j.conbuildmat.2022.128043

Wang, X., Guo, Y., Su, J., Zhang, X., Wang, Y., Tan, Y., 2018. Fabrication and Characterization of Novel Electrothermal Self-Healing Microcapsules with Graphene/Polymer Hybrid

Shells for Bitumenious Material. NANOMATERIALS 8. https://doi.org/10.3390/nano8060419

Wang, Z., Li, Z., Li, G., Liu, H., Yang, L., 2018. Evaluation of Rejuvenator on Softening, Toughness, and Diffusion Ability for Lab-Aged SBS Modified Asphalt, in: Wang, L., Ling, J., Ling, J., Zhu, H., Gong, H., Huang, B. (Eds.), . Presented at the TRANSPORTATION RESEARCH CONGRESS 2016: INNOVATIONS IN TRANSPORTATION RESEARCH INFRASTRUCTURE: PROCEEDINGS OF THE TRANSPORTATION RESEARCH CONGRESS 2016, pp. 49–60.

Xiao, Y., Li, C., Wan, M., Zhou, X., Wang, Y., Wu, S., 2017. Study of the Diffusion of Rejuvenators and Its Effect on Aged Bitumen Binder. Appl. Sci.-BASEL 7. https://doi.org/10.3390/app7040397

Xu, H., Wu, S., Chen, A., Zou, Y., 2022a. Influence of erosion factors (time, depths and environment) on induction heating asphalt concrete and its mechanism. J. Clean. Prod. 363, 132521. https://doi.org/10.1016/j.jclepro.2022.132521

Xu, H., Wu, S., Chen, A., Zou, Y., Yang, C., Cui, P., 2022b. Study on preparation and characterization of a functional porous ultra-thin friction course (PUFC) with recycled steel slag as aggregate. J. Clean. Prod. 380, 134983. https://doi.org/10.1016/j.jclepro.2022.134983

Xu, J., Ma, B., Mao, W., Si, W., Wang, X., 2023. Review of interfacial adhesion between asphalt and aggregate based on molecular dynamics. Constr. Build. Mater. 362. https://doi.org/10.1016/j.conbuildmat.2022.129642

Xu, M., Yi, J., Feng, D., Huang, Y., 2019. Diffusion characteristics of asphalt rejuvenators based on molecular dynamics simulation. Int. J. PAVEMENT Eng. 20, 615–627. https://doi.org/10.1080/10298436.2017.1321412

Xu, S., Liu, X., Tabakovic, A., Schlangen, E., 2021. Experimental Investigation of the Performance of a Hybrid Self-Healing System in Porous Asphalt under Fatigue Loadings. Materials 14. https://doi.org/10.3390/ma14123415

Yang, C., Wu, S., Cui, P., Amirkhanian, S., Zhao, Z., Wang, F., Zhang, L., Wei, M., Zhou, X., Xie, J., 2022a. Performance characterization and enhancement mechanism of recycled asphalt mixtures involving high RAP content and steel slag. J. Clean. Prod. 336, 130484. https://doi.org/10.1016/j.jclepro.2022.130484

Yang, C., Wu, S., Xie, J., Amirkhanian, S., Liu, Q., Zhang, J., Xiao, Y., Zhao, Z., Xu, H., Li, N., Wang, F., Zhang, L., 2022b. Enhanced induction heating and self-healing performance of recycled asphalt mixtures by incorporating steel slag. J. Clean. Prod. 366, 132999. https://doi.org/10.1016/j.jclepro.2022.132999

Yang, C., Wu, S., Xie, J., Amirkhanian, S., Zhao, Z., Xu, H., Wang, F., Zhang, L., 2023. Development of blending model for RAP and virgin asphalt in recycled asphalt mixtures via a micron-Fe3O4 tracer. J. Clean. Prod. 383, 135407. https://doi.org/10.1016/j.jclepro.2022.135407

You, L., Spyriouni, T., Dai, Q., You, Z., Khanal, A., 2020. Experimental and molecular dynamics simulation study on thermal, transport, and rheological properties of asphalt. Constr. Build. Mater. 265. https://doi.org/10.1016/j.conbuildmat.2020.120358

Yu, X., Liu, Q., Wan, P., Song, J., Wang, H., Zhao, F., Wang, Y., Wu, J., 2022. Effect of Ageing on Self-Healing Properties of Asphalt Concrete Containing Calcium Alginate/Attapulgite

Composite Capsules. MATERIALS 15. https://doi.org/10.3390/ma15041414

Zhan, Y., Wu, H., Song, W., Zhu, L., 2022. Molecular Dynamics Study of the Diffusion between Virgin and Aged Asphalt Binder. COATINGS 12. https://doi.org/10.3390/coatings12030403

Zhang, L., Liu, Q., Li, H., Norambuena-Contreras, J., Wu, S., Bao, S., Shu, B., 2019. Synthesis and characterization of multi-cavity Ca-alginate capsules used for self-healing in asphalt mixtures. Constr. Build. Mater. 211, 298–307. https://doi.org/10.1016/j.conbuildmat.2019.03.224

Zhao, Y., Chen, M., Zhang, X., Wu, S., Zhou, X., Jiang, Q., 2022. Effect of chemical component characteristics of waste cooking oil on physicochemical properties of aging asphalt. Constr. Build. Mater. 344. https://doi.org/10.1016/j.conbuildmat.2022.128236

Zhao, Z., Wu, S., Xie, J., Yang, C., Wang, F., Li, N., Liu, Q., Amirkhanian, S., 2024. Effect of direct addition of asphalt rubber pellets on mixing, performance and VOCs of asphalt mixtures. Constr. Build. Mater. 411, 134494. https://doi.org/10.1016/j.conbuildmat.2023.134494

Ziari, H., Hajiloo, M., Ayar, P., 2022. Influence of Recycling Agents Addition Methods on Asphalt Mixtures Properties Containing Reclaimed Asphalt Pavement (RAP). SUSTAINABILITY 14. https://doi.org/10.3390/su142416717

Zou, Y., Amirkhanian, S., Xu, S., Li, Y., Wang, Y., Zhang, J., 2021. Effect of different aqueous solutions on physicochemical properties of asphalt binder. Constr. Build. Mater. 286, 122810. https://doi.org/10.1016/j.conbuildmat.2021.122810

Zou, Y., Gao, Y., Chen, A., Wu, S., Li, Y., Xu, H., Wang, H., Yang, Y., Amirkhanian, S., 2024. Adhesion failure mechanism of asphalt-aggregate interface under an extreme saline environment: A molecular dynamics study. Appl. Surf. Sci. 645, 158851. https://doi.org/10.1016/j.apsusc.2023.158851